Alexandria Engineering Journal (2022) 61, 4779–4791

HOSTED BY

Alexandria University

Alexandria Engineering Journal

www.elsevier.com/locate/aej
www.sciencedirect.com

A new comparative study on the general fractional model of COVID-19 with isolation and quarantine effects

D. Baleanu [a,b,c], M. Hassan Abadi [d], A. Jajarmi [e,*], K. Zarghami Vahid [f], J.J. Nieto [g]

[a] Department of Mathematics, Faculty of Arts and Sciences, Çankaya University, 06530 Ankara, Turkey
[b] Institute of Space Sciences, P.O. Box, MG-23, R 76900 Magurele-Bucharest, Romania
[c] Department of Medical Research, China Medical University Hospital, China Medical University, Taichung, Taiwan
[d] Department of Mathematics, Faculty of Mathematical Science and Statistics, University of Birjand, Birjand, Iran
[e] Department of Electrical Engineering, University of Bojnord, P.O. Box, 94531-1339, Bojnord, Iran
[f] Islamic Azad University, Tehran Science and Research Branch, Tehran, Iran
[g] Instituto de Matemáticas, Universidade de Santiago de Compostela, 15782 Santiago de Compostela, Spain

Received 3 August 2021; revised 5 September 2021; accepted 13 October 2021
Available online 22 October 2021

KEYWORDS

Fractional calculus;
General fractional derivative;
COVID-19 pandemic;
Isolation and quarantine effects;
Stability analysis;
Modified predictor–corrector method

Abstract A generalized version of fractional models is introduced for the COVID-19 pandemic, including the effects of isolation and quarantine. First, the general structure of fractional derivatives and integrals is discussed; then the generalized fractional model is defined from which the stability results are derived. Meanwhile, a set of real clinical observations from China is considered to determine the parameters and compute the basic reproduction number, *i.e.*, $R_0 \approx 6.6361$. Additionally, an efficient numerical technique is applied to simulate the new model and provide the associated numerical results. Based on these simulations, some figures and tables are presented, and the data of reported cases from China are compared with the numerical findings in both classical and fractional frameworks. Our comparative study indicates that a particular case of general fractional formula provides a better fit to the real data compared to the other classical and fractional models. There are also some other key parameters to be examined that show the health of society when they come to eliminate the disease.

1. Introduction

Over the past few years, an unknown, deadly, and rapidly spreading infection called coronavirus has made worldwide fears. For the first time, coronavirus was associated with a virus family that causes infection in mammals and birds. Among humans, meanwhile, coronavirus can also cause the

* Corresponding author.
E-mail address: a.jajarmi@ub.ac.ir (A. Jajarmi).
Peer review under responsibility of Faculty of Engineering, Alexandria University.

https://doi.org/10.1016/j.aej.2021.10.030

infection of respiratory tract. Generally, coronavirus causes viral or bacterial pneumonia, respectively, either directly or indirectly. The general belief is that the 2019 coronavirus (COVID-19) is a bat-derived influenza virus; however, many controversies exist about its origin. In this case, the first question that should be asked is whether the bats are new all over the world or not, and if they are, why has this virus not been widespread earlier? Why has such a virus not been transmitted to humans earlier? A theory suggests that Chinese people ate uncooked bats, which led to the spread of this disease to people. It would be nice to go back to several African villages, where people consume fruits that were once bitten directly by bats. If this hypothesis is correct, this disease can transmit via bats. In regards to the fact that bats are the main part of dietary habits for locals, there is a possibility that locals get the virus from them. In 1981, several books were published, among which *The Eyes of Darkness* shows what the breakout of the disease would look like and how it would begin. Besides, this book claims that the virus is a bio-weapon. The date of the pandemic is also clearly stated in the book entitled *The End of the World Book*.

Mathematical models can help public health interventions by showing the likely outcome of an epidemic. In the book [1], the authors covered the concept of mathematical models in epidemiology for certain diseases such as HIV/AIDS, influenza, dengue fever, Zika virus, etc. The paper [2] investigated the impact of case-area targeted intervention and its effect on reducing cholera transmission. The other study [3] introduced vaccines to susceptible people in order to control Ebola disease spread. In [4], the power series solutions of compartmental epidemiological models were used to create alternative approaches for solving their nonlinear differential equation systems. The dynamics of COVID-19 have also been investigated by several formulas [5,6]. In [7], the COVID-19 dynamics were analyzed by using three numerical schemes in the frameworks of singular and nonsingular fractional operators. In [8], the authors developed a model that synthesized the indicators extracted from the outbreak in Wuhan (China). The COVID-19 dynamics in Italy were analyzed in [9] by the concept of mathematical modelling. Based on Tennessee State data in the United States, the study [10] presented a fractional compartmental model for the spread of COVID-19. In [11], the simulation of COVID-19 transmission in a northeastern state of Brazil was investigated through a mathematical model. The work [12] studied a new model of COVID-19 by not only applying the real-world data from Pakistan but also using the stability theory of differential equations. In [13], a new model of COVID-19 was taken into account by using a fractional operator with nonsingular kernel instead of classical derivatives, and a modified Adams–Bashforth scheme was employed to solve the model. According to the research in [14], the transmission and death rates of COVID-19 could be reduced dramatically in Ghana through mathematical modelling. Moreover, researchers used a fractional model with a lock-down function to investigate the lock-down effect on the COVID-19 transmission in Turkey [15]. In [16], the solution of a fractional COVID-19 model was studied by using Hermite wavelets, and the results were compared with those of Adams–Bashforth-Moulton predictor–corrector method. In [17], the COVID-19 was analyzed in India with fractional calculus by using an SEIR model and a q-Homotopy analysis transform technique; the existence and uniqueness of the results were also determined based on the fixed point theory. In [18], to extend the COVID-19 model, a set of real-world data was used by taking into account the isolation and quarantine effects. In [19], a stochastic COVID-19 model with Lévy noise was shown and analyzed; in all model compartments, Lévy jump perturbations and white noise were included, and the stochastic solution near the deterministic equilibrium model was used to study the dynamical stochastic properties. Another study [20] employed a fractional frequency flexible Fourier form to test the COVID-19 predictability along with nonlinear trends and fractional integration. To eradicate COVID-19, non-pharmaceutical interventions based on mathematical modelling were introduced in [21], and the threshold conditions were studied for the disease-free steady-states. Based on parametric perturbations and transition probabilities, the authors in [22] discussed the use of non-standard computations to study the stochastic pandemic model of COVID-19. The paper [23] also examined the bats-hosts-reservoir-people COVID-19 model and used a variational iteration method to derive its corresponding approximate solution.

In the past decades, scientists have made it possible to model real phenomena through fractional-order systems since such systems inherently exhibit memory effects [24,25]. As well, it was shown that fractional models are impressive in analyzing complex systems in different fields such as finance, biology, and mechanics [26–28]. Some valuable studies in the theoretical and practical aspects of fractional calculus are briefly reviewed here. In [29], by using weak topology, the existence results were presented for the Caputo fractional neutral inclusions without compactness in Banach space. Using fixed-point theorem and fractional calculus approach, the authors in [30] provided controllability results under sufficient conditions. The paper [31] introduced integro-differential equations based on Atangana-Baleanu fractional derivative with a generalized Mittag–Leffler kernel and examined the existence and uniqueness of the solutions in Banach space. In [32], non-compactness procedures and Mönch's fixed point theorem were used to investigate fractional integro-differential equations involving Hilfer fractional operators with non-local conditions. In a nonsense region, Hilfer's neutral fractional derivative provided controllability results using Mönch's method, Banach's contraction principle, fractional calculus, and semi-group property [33].

Valuable works and discussions as above motivate us to pursue further researches on the mathematical modelling of COVID-19 by considering new fractional operators and taking into account some other effective parameters like isolation and quarantine effects. To this end, first, we present an integer-order model from [18] including ordinary time derivatives; then we generalize this model in a new framework by applying the concept of general fractional operators introduced by Luchko and Yamamoto [34]. From this generalization, the stability results are derived for $R_0 < 1$. A new numerical method is also proposed for solving the obtained general fractional differential equations. In both classical and fractional frameworks, the data of reported cases from China is compared with the numerical findings of this article. Simulation results show that the general fractional model for various fractional orders and different kernel functions offers a degree of flexibility and allows us to model the complex biological system under investigation in a more precise way than the other types of fractional and classical equations. In addition, we examine

some of the key parameters and their effects on the model behavior, which could act as a control in eradicating the disease. In conclusion, this study is very useful and presents some crucial information that can help to eradicate the disease from communities as soon as possible.

This paper is classified in the following sections. The preliminary notes are introduced in Section 2. A general fractional COVID-19 model with isolation and quarantine effects is presented in Section 3. Section 4 proposes a new numerical method to simulate the model. Then the results and discussions are followed in Section 5. Finally, some concluding remarks in Section 6 close the manuscript. .

2. Preliminary notes

In this part, some preliminaries are presented about the recently introduced general fractional derivatives and integrals. According to [34], the general form of left Caputo and Riemann–Liouville fractional derivatives would, respectively, be written by

$$ {}_0{}^{C}\mathrm{D}_t^{\alpha} f(t) = \int_0^t \dot{f}(s)\mathrm{K}_{\mathrm{L}}(t-s)\,ds, \tag{1} $$

$$ {}_0\mathrm{D}_t^{\alpha} f(t) = \frac{d}{dt}\int_0^t f(s)\mathrm{K}_{\mathrm{L}}(t-s)\,ds, \tag{2} $$

in which $\alpha \in (0,1)$ is the order of fractional derivative, $f:[0,+\infty)\to\mathbb{R}$ is an absolutely continuous function with $\dot{f}\in L^1_{loc}(0,+\infty), 0\leqslant t\leqslant T<+\infty$, and $\mathrm{K_L}$ is a general kernel function that is non-negative and locally integrable on $\mathbb{R}^+$. Notice that the above general operators are linear, so we have

$$ {}_0{}^{C}\mathrm{D}_t^{\alpha}(\lambda f(t)+\mu g(t)) = \lambda\ {}_0{}^{C}\mathrm{D}_t^{\alpha} f(t) + \mu\ {}_0{}^{C}\mathrm{D}_t^{\alpha} g(t), \tag{3} $$

$$ {}_0\mathrm{D}_t^{\alpha}(\lambda f(t)+\mu g(t)) = \lambda\ {}_0\mathrm{D}_t^{\alpha} f(t) + \mu\ {}_0\mathrm{D}_t^{\alpha} g(t). \tag{4} $$

Also, under some conditions of the kernel function $\mathrm{K_L}(t)$, an entirely monotone function $\mathrm{M_L}(t)$ exists for all $t>0$ such that [34]

$$ \mathrm{K_L}(t) * \mathrm{M_L}(t) = \int_0^{\infty} \mathrm{K_L}(s)\mathrm{M_L}(t-s)\,ds = 1. \tag{5} $$

Moreover, for $f\in L^1_{loc}(0,+\infty)$, it can be written

$$ {}_0\mathrm{D}_t^{-\alpha}\left[{}_0{}^{C}\mathrm{D}_t^{\alpha} f(t)\right] = f(t) - f(0), \tag{6} $$

where ${}_0\mathrm{D}_t^{-\alpha}$ represents the general form of Riemann–Liouville fractional integral defined by

$$ {}_0\mathrm{D}_t^{-\alpha} f(t) = \int_0^t f(s)\mathrm{M_L}(t-s)\,ds. \tag{7} $$

Following the same concept as above, the right Caputo and Riemann–Liouville fractional derivatives could be, respectively, stated by

$$ {}_t{}^{C}\mathrm{D}_T^{\alpha} f(t) = \int_t^T \dot{f}(s)\mathrm{K_R}(s-t)\,ds, \tag{8} $$

$$ {}_t\mathrm{D}_T^{\alpha} f(t) = \frac{d}{dt}\int_t^T f(s)\mathrm{K_R}(s-t)\,ds, \tag{9} $$

and the right-sided Riemann–Liouville fractional integral would be described as

$$ {}_t\mathrm{D}_T^{-\alpha} f(t) = \int_t^T f(s)\mathrm{M_R}(s-t)\,ds. \tag{10} $$

It could be noticeable that the above generalization coincides with another one in [35]; hence, the integration by parts formula, according to the consequences in [35], is also fulfilled by the aforesaid fractional operators as follows

$$ \int_0^T f(s)\,{}_0\mathrm{D}_s^{\alpha} g(s)\,ds = \int_0^T g(s)\,{}_s{}^{C}\mathrm{D}_T^{\alpha} f(s)\,ds, \tag{11} $$

$$ \int_0^T f(s)\,{}_0{}^{C}\mathrm{D}_s^{\alpha} g(s)\,ds = \int_0^T g(s)\,{}_s\mathrm{D}_T^{\alpha} f(s)\,ds. \tag{12} $$

Now, three particular cases are introduced here according to the recent definitions. First, the general kernel $\mathrm{K_L}(t)$ is set as $\mathrm{K_L}(t)=\frac{t^{-\alpha}}{\Gamma(1-\alpha)}$; thus, the power function $\mathrm{M_L}(t)=\frac{t^{\alpha-1}}{\Gamma(\alpha)}$ constitutes the associated kernel for the integral operator (7). Consequently, the Eqs. (1) and (2) decrease to the conventional Caputo and Reimann-Liouville derivatives, respectively, and the Eq. (7) becomes the Riemann–Liouville integral [36]. Second, the kernel $\mathrm{K_L}(t)=\frac{\mathrm{M}(\alpha)}{1-\alpha}\mathrm{E}_{\alpha}\left(\frac{-\alpha}{1-\alpha}t^{\alpha}\right)$ would be considered in which E_{α} and $\mathrm{M}(\alpha)$ are, respectively, the Mittag–Leffler and normalization functions such that $\mathrm{M}(0)=\mathrm{M}(1)=1$. Then by applying the Laplace transformation, we achieve the kernel $\mathrm{M_L}(t)$ as

$$ \mathrm{M_L}(t) = \frac{1-\alpha}{\mathrm{M}(\alpha)}\delta(t) + \frac{\alpha}{\mathrm{M}(\alpha)\Gamma(\alpha)}t^{\alpha-1}. \tag{13} $$

Therefore, the Atangana-Baleanu (AB)-Caputo and AB-Riemann–Liouville derivatives are, respectively, recovered from the Eqs. (1) and (2), and the AB fractional integral is acquired by [37]

$$ {}_0\mathrm{D}_t^{-\alpha} f(t) = \frac{\alpha}{\mathrm{M}(\alpha)\Gamma(\alpha)}\int_0^t (t-s)^{\alpha-1} f(s)\,ds + \frac{1-\alpha}{\mathrm{M}(\alpha)} f(t). \tag{14} $$

Finally, the Caputo-Fabrizio (CF) derivative is formulated by setting $\mathrm{K_L}(t)=\frac{\mathrm{M}(\alpha)}{1-\alpha}\exp\left(\frac{-\alpha}{1-\alpha}t\right)$ in which the kernel is an exponential function. Furthermore, $\mathrm{M}(\alpha)$ would be the normalization function satisfying $\mathrm{M}(0)=\mathrm{M}(1)=1$ [38–40].

3. Mathematical modelling

In this section, the new model of COVID-19 with isolation and quarantine effects is analyzed in both integer- and fractional-order frameworks. As a part of this section, the non-negativity of the solution is investigated. Then the feasible region is presented, which is shown to be positively invariant. Finally, by introducing the basic reproduction number, the equilibrium points and their stability are explored.

3.1. Integer-order case

The threat posed by COVID-19 to millions of people worldwide is becoming a real threat and a severe health risk. Isolation and quarantine could be introduced as effective and practical solutions to decline and eradicate the disease transmission rate. Coronavirus can spread through people who have clinical symptoms and are vulnerable to infection; thus, they must be quarantined and isolated for a short period because of their high-risk position. In addition, this issue also

includes asymptomatic infected patients who play a role in the infection cycle without displaying any symptoms, causing a new disease possible. In the new model developed in this section, the notation $P(t)$ indicates the total number of population with seven sub-categories, *i.e.*, susceptible people $S(t)$, vulnerable individuals $V(t)$ who do not show the disease symptoms, clinically symptomatic infected people $I(t)$, asymptomatic infected persons $A(t)$ (with hardly any clinical signs), quarantined people $K(t)$, under treatment individuals $U(t)$, and people who are recuperated $R(t)$. The seafood market $M(t)$ is mainly responsible for this infection because people, who visit the markets and purchase the food, get infected and spread it throughout the environment. As a result, an ordinary differential equations system, which describes the disease, could be derived by applying the above assumptions as below [18]

$$\begin{aligned}
\frac{dS(t)}{dt} &= \beta - \xi S(t) - \upsilon(t)S(t),\\
\frac{dV(t)}{dt} &= -((1-\omega)\sigma_1 + \omega\sigma_2 + \xi + \kappa_v)V(t) + \upsilon(t)S(t),\\
\frac{dI(t)}{dt} &= -(\rho_\iota + \xi + \xi_\iota + \eta_\iota)I(t) + (1-\omega)\sigma_1 V(t),\\
\frac{dA(t)}{dt} &= -(\rho_a + \xi)A(t) + \omega\sigma_2 V(t),\\
\frac{dK(t)}{dt} &= -(\xi + \rho_\kappa + \eta_\kappa)K(t) + \kappa_v V(t),\\
\frac{dU(t)}{dt} &= -(\xi + \rho_u + \xi_u)U(t) + \eta_\iota I(t) + \eta_\kappa K(t),\\
\frac{dR(t)}{dt} &= -\xi R(t) + \rho_\iota I(t) + \rho_a A(t) + \rho_\kappa K(t) + \rho_u U(t),\\
\frac{dM(t)}{dt} &= -\tau_m M(t) + \tau_a A(t) + \tau_\iota I(t),
\end{aligned} \tag{15}$$

in which

$$\upsilon(t) = \frac{\theta_1(I(t) + \phi A(t))}{P(t)} + \theta_2 M(t). \tag{16}$$

The infected people with clinically symptomatic or without clinical symptoms, as well as the infected individuals of seafood markets $(I(t), A(t), M(t))$ can infect the susceptible people to the disease, which is shown as $\upsilon(t)$. For susceptible individuals, the corresponding birth rate is β, and the human mortality rate can be measured by ξ. Healthy people would become infectious after exposure to the infected and asymptomatically infected individuals at the rate θ_1, whereas the transmissibility factor is denoted by ϕ. The number of people who are affected as a result of visiting seafood markets is increased by θ_2. The parameter ω generates the asymptomatic infection. The periods of incubation are represented by σ_1 and σ_2. The parameter κ_v represents the number of individuals who have been exposed to the infection and are being quarantined. The parameters ρ_a and ρ_ι refer to the percentage recuperation of asymptomatic infection and infection, respectively. Also, the parameters ρ_u and ρ_κ are, respectively, the recuperation of hospitalized and quarantined people. The disease-related death rates of hospitalized and infected people are represented by ξ_u and ξ_ι, respectively. In addition, the hospitalization rate for the infected and quarantine individuals has been calculated with η_ι and η_κ, respectively. Not only are the parameters τ_ι and τ_a, respectively, shown the infections came from the infected and asymptomatically infected people at seafood markets, but also the parameter τ_m represents the removed infected individuals from the markets.

3.2. Non-negativity of the solution

Lemma 3.1. *Let $\Delta(t)$ be the state vector of the model (15), i.e.,*

$$\Delta(t) = (S(t), V(t), I(t), A(t), K(t), U(t), R(t), M(t)),$$

and $\Delta(0) = (S_0, V_0, I_0, A_0, K_0, U_0, R_0, M_0) \geqslant 0$ be the non-negative initial state vector. Then the model (15) has a non-negative solution for any time $t > 0$. Moreover, we have $\lim_{t\to\infty} P(t) \leqslant \frac{\beta}{\xi}$ where $P(t)$ would be the total population computed by $P(t) = S(t) + V(t) + I(t) + A(t) + K(t) + U(t) + R(t)$.

Proof. Let us take into account

$$t_{sup} = sup\{t > 0 : \Delta(t) > 0\}.$$

Thus, $t_{sup} > 0$. The first equation of the model (15) leads to the following relation

$$\frac{dS(t)}{dt} = \beta - \xi S(t) - \upsilon(t)S(t) = \beta - S(t)(\xi + \upsilon(t)), \tag{17}$$

where $\upsilon(t) = \frac{\theta_1(I(t)+\phi A(t))}{P(t)} + \theta_2 M(t)$. Thus, the Eq. (17) can be written as

$$\begin{aligned}
&\frac{d}{dt}\left\{S(t)\exp\left(\xi t + \int_0^{t_{sup}} \upsilon(s)ds\right)\right\}\\
&\quad = \beta\exp\left(\xi t + \int_0^{t_{sup}} \upsilon(s)ds\right).
\end{aligned} \tag{18}$$

Therefore,

$$\begin{aligned}
&S(t_{sup})\exp\left(\xi t_{sup} + \int_0^{t_{sup}} \upsilon(s)ds\right) - S(0)\\
&\quad = \int_0^{t_{sup}} \beta\exp\left(\xi y + \int_0^{y} \upsilon(\zeta)d\zeta\right)dy,
\end{aligned} \tag{19}$$

such that

$$\begin{aligned}
S(t_{sup}) &= S(0)\exp\left\{-\left(\xi t_{sup} + \textstyle\int_0^{t_{sup}} \upsilon(s)ds\right)\right\}\\
&\quad + \exp\left\{-\left(\xi t_{sup} + \textstyle\int_0^{t_{sup}} \upsilon(s)ds\right)\right\}\\
&\quad \times \textstyle\int_0^{t_{sup}} \beta\exp\left(\xi y + \int_0^{y} \upsilon(\zeta)d\zeta\right)dy > 0.
\end{aligned} \tag{20}$$

We can follow a similar strategy for the remaining equations in the system (15) to prove $\Delta(t) > 0$ for all $t > 0$. For further assertion, consider that the initial conditions satisfy $0 < S_0, V_0, I_0, A_0, K_0, U_0, R_0 \leqslant P(t)$. In the system (15), all the equations except the last one are added together; thus, we obtain

$$\frac{dP(t)}{dt} = \beta - \xi P(t) - \xi_\iota I(t) - \xi_u U(t) \leqslant \beta - \xi P(t).$$

Consequently, we have

$$\lim_{t\to\infty} P(t) \leqslant \frac{\beta}{\xi}.$$

□

In the following, we present an invariant region for the system (15). Let the feasible region Z be specified by

$$Z = \left\{(S, V, I, A, K, U, R) \in \mathbb{R}_+^7 : P(t) \leqslant \frac{\beta}{\xi}, \quad M \in \mathbb{R}_+ : M(t) \leqslant \frac{\beta}{\xi}\frac{\tau_\iota + \tau_a}{\tau_m}\right\}. \tag{21}$$

Lemma 3.2. *Consider nonnegative initial conditions for the system (15); then the region Z is positively invariant.*

Proof. Again, all the equations in (15) except the last one are added together; thus, we get

$$\frac{dP(t)}{dt} = \beta - \xi P(t) - \xi_\iota I(t) - \xi_u U(t) \leqslant \beta - \xi P(t).$$

If $P(0) \leqslant \frac{\beta}{\xi}$, then $\frac{dP(t)}{dt} \leqslant 0$. Therefore, $P(t) \leqslant P(0)e^{-\xi t} + \frac{\beta}{\xi}(1 - e^{-\xi t})$. Hence, the region Z is positively invariant. Furthermore, either $P(t)$ tends asymptomatically toward $\frac{\beta}{\xi}$ or the solution enters Z in a finite time if we have $P(0) < \frac{\beta}{\xi}$ and $M(0) < \frac{\beta}{\xi}\frac{\tau_\iota+\tau_a}{\tau_m}$. This means that all the solutions in $\mathbb{R}_+^7$ are attracted by the region given by Z. □

3.3. Fractional-order case

In this section, a general fractional derivative, which is presented in Section 2, would be applied to modify the COVID-19 model dynamics (15). Thus, the following new and general fractional model is available

$$\begin{aligned}
\frac{1}{\sigma^{1-\alpha}}{}_0{}^C\mathrm{D}_t^\alpha S(t) &= \beta - \xi S(t) - \upsilon(t)S(t),\\
\frac{1}{\sigma^{1-\alpha}}{}_0{}^C\mathrm{D}_t^\alpha V(t) &= -((1-\omega)\sigma_1 + \omega\sigma_2 + \xi + \kappa_v)V(t) + \upsilon(t)S(t),\\
\frac{1}{\sigma^{1-\alpha}}{}_0{}^C\mathrm{D}_t^\alpha I(t) &= -(\rho_\iota + \xi + \xi_\iota + \eta_\iota)I(t) + (1-\omega)\sigma_1 V(t),\\
\frac{1}{\sigma^{1-\alpha}}{}_0{}^C\mathrm{D}_t^\alpha A(t) &= -(\rho_a + \xi)A(t) + \omega\sigma_2 V(t),\\
\frac{1}{\sigma^{1-\alpha}}{}_0{}^C\mathrm{D}_t^\alpha K(t) &= -(\xi + \rho_\kappa + \eta_\kappa)K(t) + \kappa_v V(t),\\
\frac{1}{\sigma^{1-\alpha}}{}_0{}^C\mathrm{D}_t^\alpha U(t) &= -(\xi + \rho_u + \xi_u)U(t) + \eta_\iota I(t) + \eta_\kappa K(t),\\
\frac{1}{\sigma^{1-\alpha}}{}_0{}^C\mathrm{D}_t^\alpha R(t) &= -\xi R(t) + \rho_\iota I(t) + \rho_a A(t) + \rho_\kappa K(t) + \rho_u U(t),\\
\frac{1}{\sigma^{1-\alpha}}{}_0{}^C\mathrm{D}_t^\alpha M(t) &= -\tau_m M(t) + \tau_\iota I(t) + \tau_a A(t),
\end{aligned} \tag{22}$$

in which

$$\upsilon(t) = \frac{\theta_1(I(t) + \phi A(t))}{P(t)} + \theta_2 M(t), \tag{23}$$

together with nonnegative initial conditions. According to the formula (1), the expression ${}_0{}^C\mathrm{D}_t^\alpha$ represents the general left Caputo fractional derivative, and α shows the fractional order. Also, to ensure that the above-mentioned fractional equations are dimensionally matched on both sides, the coefficient $\frac{1}{\sigma^{1-\alpha}}$, including the auxiliary parameter σ, is considered [41].

3.3.1. Equilibrium points and stability

Let P_0 denote the disease-free equilibrium point by means of the model (22). Then we have

$$P_0 = \{S(0), 0, 0, 0, 0, 0, 0, 0\} = \left\{\frac{\beta}{\xi}, 0, 0, 0, 0, 0, 0, 0\right\}.$$

The basic reproduction number of the model (22) could be obtained by means of a next-generation matrix [42] as follows

$$F = \sigma^{1-\alpha}\begin{bmatrix} 0 & \theta_1 & \phi\theta_1 & 0 & 0 & \frac{\beta\theta_2}{\xi} \\ 0 & 0 & 0 & 0 & 0 & 0 \\ 0 & 0 & 0 & 0 & 0 & 0 \\ 0 & 0 & 0 & 0 & 0 & 0 \\ 0 & 0 & 0 & 0 & 0 & 0 \\ 0 & 0 & 0 & 0 & 0 & 0 \end{bmatrix},$$

$$V = \sigma^{1-\alpha}\begin{bmatrix} q_1 & 0 & 0 & 0 & 0 & 0 \\ (\omega-1)\sigma_1 & q_2 & 0 & 0 & 0 & 0 \\ -\omega\sigma_2 & 0 & q_3 & 0 & 0 & 0 \\ -\kappa_v & 0 & 0 & q_4 & 0 & 0 \\ 0 & -\eta_\iota & 0 & -\eta_\kappa & q_5 & 0 \\ 0 & -\tau_\iota & -\tau_a & 0 & 0 & \tau_m \end{bmatrix},$$

$$\begin{aligned}
R_0 &= \rho\left(FV^{-1}\right)\\
&= \left(\frac{\omega q_2\sigma_2(\theta_2\beta\tau_a + \theta_1\xi\tau_m\phi) + (1-\omega)q_3\sigma_1(\theta_2\beta\tau_\iota + \theta_1\xi\tau_m)}{q_1q_2q_3\xi\tau_m}\right)\\
&= \underbrace{\frac{\theta_2\omega\beta\sigma_2\tau_a}{q_1q_3\xi\tau_m}}_{R_1} + \underbrace{\frac{\theta_1\omega\sigma_2\phi}{q_1q_3}}_{R_2} + \underbrace{\frac{\theta_2(1-\omega)\beta\tau_\iota\sigma_1}{q_1q_2\xi\tau_m}}_{R_3} + \underbrace{\frac{\theta_1(1-\omega)\sigma_1}{q_1q_2}}_{R_4},
\end{aligned}$$

where

$$\begin{aligned}
q_1 &= \kappa_v + \omega\sigma_2 + (1-\omega)\sigma_1 + \xi,\\
q_2 &= \eta_\iota + \xi + \xi_\iota + \rho_\iota,\\
q_3 &= \xi + \rho_a,\\
q_4 &= \eta_\kappa + \xi + \rho_\kappa,\\
q_5 &= \xi + \xi_u + \rho_u.
\end{aligned}$$

The next step is to show that the model (22) is stable locally.

Theorem 3.1. If $R_0 < 1$ at the equilibrium point P_0, then the system (15) would be locally asymptotically stable.

Proof. First, we would calculate a Jacobian matrix of the model (22) at P_0

$$J_{P_0} = \sigma^{1-\alpha}\begin{bmatrix} -\xi & 0 & -\theta_1 & -\phi\theta_1 & 0 & 0 & 0 & -\frac{\beta\theta_2}{\xi} \\ 0 & -q_1 & \theta_1 & \phi\theta_1 & 0 & 0 & 0 & \frac{\beta\theta_2}{\xi} \\ 0 & (1-\omega)\sigma_1 & -q_2 & 0 & 0 & 0 & 0 & 0 \\ 0 & \omega\sigma_2 & 0 & -q_3 & 0 & 0 & 0 & 0 \\ 0 & \kappa_v & 0 & 0 & -q_4 & 0 & 0 & 0 \\ 0 & 0 & \eta_\iota & 0 & \eta_\kappa & -q_5 & 0 & 0 \\ 0 & 0 & \rho_\iota & \rho_a & \rho_\kappa & \rho_u & -\xi & 0 \\ 0 & 0 & \tau_\iota & \tau_a & 0 & 0 & 0 & -\tau_m \end{bmatrix}, \tag{24}$$

whose eigenvalues $-\mu, -\mu, -q_4$, and $-q_5$ have negative real parts. Four other eigenvalues could also be found based on the equation

$$\lambda^4 + a_3\lambda^3 + a_2\lambda^2 + a_1\lambda + a_0 = 0, \tag{25}$$

where

$$\begin{aligned} a_0 &= q_1q_2q_3\tau_m(1-R_0),\\ a_1 &= q_1q_2q_3(1-R_4) + q_1q_3\tau_m(1-R_1) + q_1q_2\tau_m(1-R_3)\\ &\quad + q_2q_3\tau_m - \theta_1(\omega q_2\sigma_2\phi + \tau_m(\omega\sigma_2\phi + (1-\omega)\sigma_1)),\\ a_2 &= q_1q_3(1-R_2) + q_1q_2(1-R_4) + (q_1+q_2+q_3)\tau_m + q_2q_3,\\ a_3 &= q_1 + q_2 + q_3 + \tau_m. \end{aligned} \tag{26}$$

It is easy to show that the coefficients $a_i, i = 1, 2, 3$, are non-negative, and a_0 is non-negative when $R_0 < 1$. Moreover, the Rough-Hurtwiz criterion $a_1a_2a_3 - a_3^2a_0 - a_1^2 > 0$ is satisfied. Also, the Rough-Hurtwiz conditions hold if $R_0 < 1$, so the system (22) could be asymptotically stable at the disease-free steady-state P_0 if $R_0 < 1$. □

At the endemic point, the equilibrium is then obtained by

$$\begin{cases} S^* = \frac{\beta^*}{\upsilon+\xi},\\ V^* = \frac{\upsilon^* S^*}{q_1},\\ I^* = \frac{(1-\omega)\sigma_1 V^*}{q_2},\\ A^* = \frac{\omega\sigma_2 V^*}{q_3},\\ K^* = \frac{\kappa_v V^*}{q_4},\\ U^* = \frac{\eta_\iota I^* + \eta_\kappa K^*}{q_5},\\ R^* = \frac{\rho_a A^* + \rho_u U^* + \rho_\iota I^* + \rho_\kappa K^*}{\xi},\\ M^* = \frac{\tau_a A^* + \tau_\iota I^*}{\tau_m}. \end{cases} \tag{27}$$

The above result can be inserted into

$$\upsilon(t) = \frac{\theta_1(I(t) + \phi A(t))}{P(t)} + \theta_2 M(t).$$

Then

$$F(\lambda^*) = b_2(\lambda^*)^2 + b_1\lambda^* + b_0,$$

in which

$$\begin{aligned} b_0 &= q_1^2q_2^2q_3^2q_4q_5\xi^2\tau_m(1-R_0),\\ b_1 &= q_1q_2q_3\xi\tau_m(q_3(\kappa_v q_2(\eta_\kappa(\xi+\rho_u) + q_5(\xi+\rho_\kappa)) + q_4q_8)\\ &\quad + \omega q_2q_4q_5\sigma_2(-\theta\phi + \xi + \rho_a))\\ &\quad + \theta_2q_7\beta((1-\omega)q_3\tau_\iota\sigma_1 - \omega q_2\sigma_2\tau_a) + q_1^2q_2^2q_4q_5q_3^2\xi\tau_m,\\ b_2 &= q_1q_2q_3\tau_m(q_3(\kappa_v q_2(\eta_\kappa(\xi+\rho_u) + q_5(\xi+\rho_\kappa))q_4q_6)\\ &\quad + \omega q_2q_4q_5\sigma_2(\xi+\rho_a)), \end{aligned}$$

and

$$\begin{aligned} q_6 &= \eta_\iota(1-\omega)\sigma_1(\xi+\rho_u) + q_5((1-\omega)\sigma_1(\xi+\rho_\iota) + q_2\xi),\\ q_7 &= q_3(-\kappa_v q_2(\eta_\kappa(\xi+\rho_u) + q_5(\xi+\rho_\kappa)) - q_4q_6) - \omega q_2q_4q_5\sigma_2(\xi+\rho_a),\\ q_8 &= \eta_\iota(1-\omega)\sigma_1(\xi+\rho_u) + q_5((1-\omega)\sigma_1(-\theta_1+\xi+\rho_\iota) + q_2\xi). \end{aligned}$$

In this case, $b_2 > 0, b_0$ is negative if $R_0 > 1$, and it is positive when $R_0 < 1$. Therefore, the sign of b_0 depends on the value of R_0. The above discussion is summarized in the sequel:

Theorem 3.2. *The following information describes the system (22):*

1. *A unique endemic equilibrium exists when $b_0 < 0$ and $R_0 > 1$.*
2. *A unique endemic equilibrium occurs if $b_1 < 0$ and $b_0 = 0$.*
3. *It follows that there exist two endemic equilibria if $b_1 < 0, b_0 > 0$, and their discriminant is positive.*
4. *Otherwise, there are no possible equilibria.*

From item 1 of Theorem 3.2, it is obvious that a unique positive endemic equilibrium exists for $R_0 > 1$. When $R_0 < 1$, item 3 of Theorem 3.2 provides backward bifurcation possibility.

4. Numerical method

This section proposes an efficient method for solving the system of general fractional Eq. (22) numerically. To this aim, the time interval $[0, T]$ is partitioned into N equal subintervals by $t_k = kh, 0 \leqslant k \leqslant N$, as the mesh points, where the step size is $h = \frac{T}{N}$, and N is a non-negative integer. We consider the notations $S_{k+1}, V_{k+1}, I_{k+1}, A_{k+1}, K_{k+1}, U_{k+1}, R_{k+1}$, and M_{k+1} to estimate the approximate values of $S(t_k), V(t_k), I(t_k), A(t_k), K(t_k), U(t_k), R(t_k)$, and $M(t_k)$, respectively. Then a predictor–corrector method is utilized to solve the equations in (22) forward-in-time.

4.1. Description of the method

In the following, a Volterra integral equation is expressed by applying the general fractional integral (7) to each side of the first equation in (22)

$$S(t) = S_0 + \int_0^t F(S(s))\mathrm{M_L}(t-s)\,ds, \tag{28}$$

where $F(S(t)) := \sigma^{1-\alpha}(\beta - \xi S(t) - \upsilon(t)S(t))$. The next equation is the result of replacing t by t_{k+1} in the Eq. (28)

$$S_{k+1} = S_0 + \int_0^{t_{k+1}} F(S(s))\mathrm{M_L}(t_{k+1}-s)\,ds. \tag{29}$$

Table 1 Fitted and estimated values for the parameters in the model (22) [18].

Parameters	Values
β	$\xi \times P(0)$
ξ	$\frac{1}{76.79\times365}$
ξ_ι	0.0002
ξ_u	0.01
θ_1	0.003
θ_2	0.00000034002
ϕ	0.004
ω	0.21003
σ_1	0.00001111
σ_2	0.0180322
ρ_ι	0.00023
ρ_a	0.19
ρ_κ	0.1
ρ_u	0.2
τ_ι	0.00101
τ_a	0.0214
τ_m	0.23008
κ_v	0.1223
η_ι	0.0005
η_κ	0.06

Then the trapezoidal quadrature formula can be used to approximate the integration part in (29)

$$\int_0^{t_{k+1}} F(S(s))\mathrm{M_L}(t_{k+1}-s)\,ds \approx \int_0^{t_{k+1}} \widehat{F}_{k+1}(s)\mathrm{M_L}(t_{k+1}-s)\,ds, \tag{30}$$

where the interpolation polynomial $\widehat{F}(S_{k+1}(s))$ is piecewise linear and calculated from

$$\widehat{F}_{k+1}(s)\Big|_{s\in[t_j,t_{j+1}]} \approx \frac{t_{j+1}-s}{t_{j+1}-t_j}F(S_j) + \frac{s-t_j}{t_{j+1}-t_j}F(S_{j+1}), \qquad 0 \leqslant j \leqslant k. \tag{31}$$

By applying the Eq. (31) in (30), we obtain

$$\int_0^{t_{k+1}} F(S(s))\mathrm{M_L}(t_{k+1}-s)\,ds \approx \sum_{j=0}^{k} F(S_j)a_{k+1,j} + F(S_{j+1})b_{k+1,j} = \sum_{j=0}^{k+1} c_{k+1,j}F(S_j), \tag{32}$$

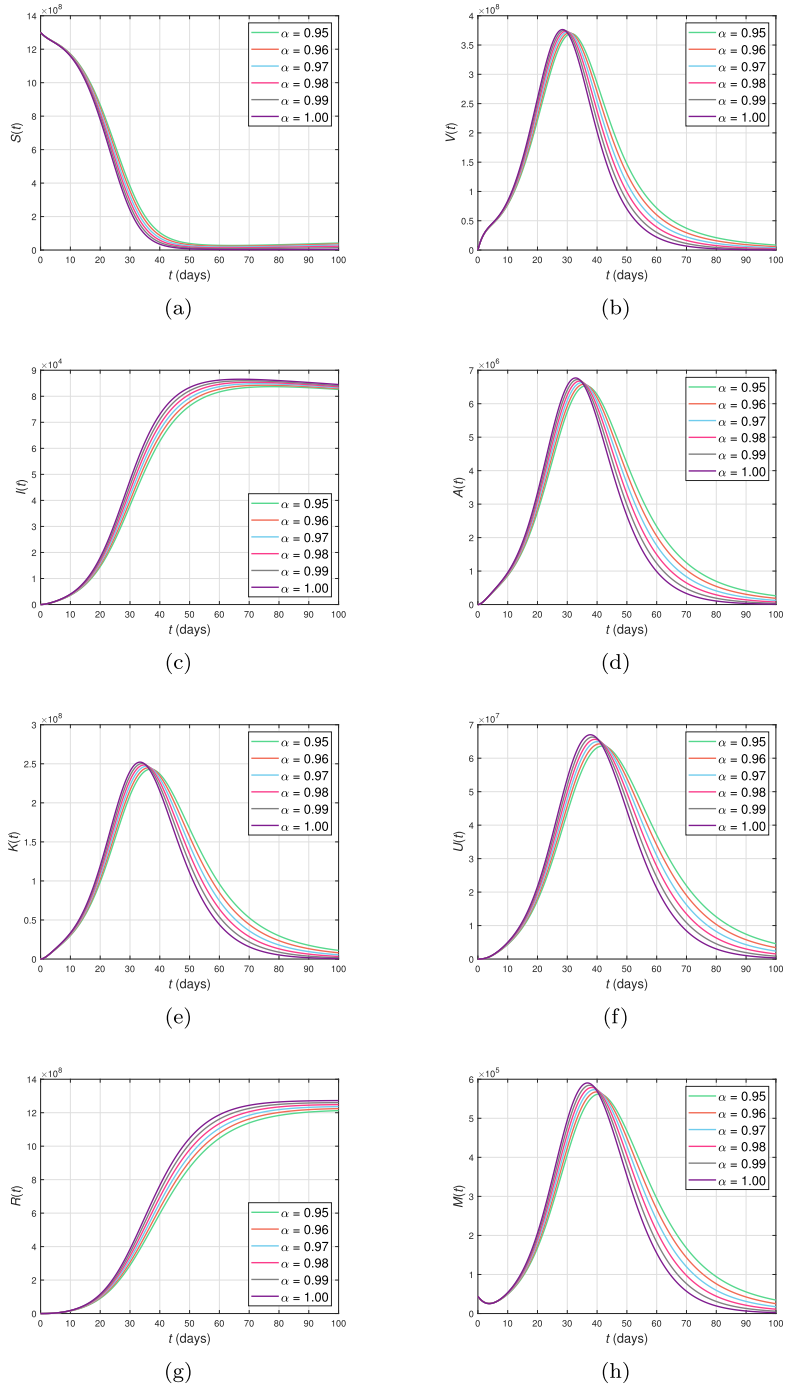

Fig. 1 The dynamics of the model (22) with a power law kernel.

in which

$$\begin{aligned} a_{k+1,j} &= \tfrac{1}{h}\int_{t_j}^{t_{j+1}} (t_{j+1}-s)\mathrm{M_L}(t_{k+1}-s)\,ds, \\ b_{k+1,j} &= \tfrac{1}{h}\int_{t_j}^{t_{j+1}} (s-t_j)\mathrm{M_L}(t_{k+1}-s)\,ds, \\ c_{k+1,j} &= \begin{cases} a_{k+1,0}, & j=0, \\ a_{k+1,j}+b_{k+1,j-1}, & 1\leqslant j\leqslant k, \\ b_{k+1,k}, & j=k+1. \end{cases} \end{aligned} \tag{33}$$

Consequently, the corrector formula for the first equation of (22) is introduced as follows

$$S_{k+1} = S_0 + c_{k+1,k+1}F\left(S_{k+1}^p\right) + \sum_{j=0}^{k} c_{k+1,j}F\left(S_j\right), \tag{34}$$

where from the predictor equation, S_{k+1}^p is known and computed hereinafter. For this purpose, instead of Eq. (31), the approximation $\widehat{F}_{k+1}(s)\Big|_{s\in[t_j,t_{j+1}]} \approx F\left(S_j\right)$ (as defined by the product rectangle rule) is employed for the integration parts in (29) and (30). Thus, the following result is obtained, instead of Eq. (32), by using this approximation

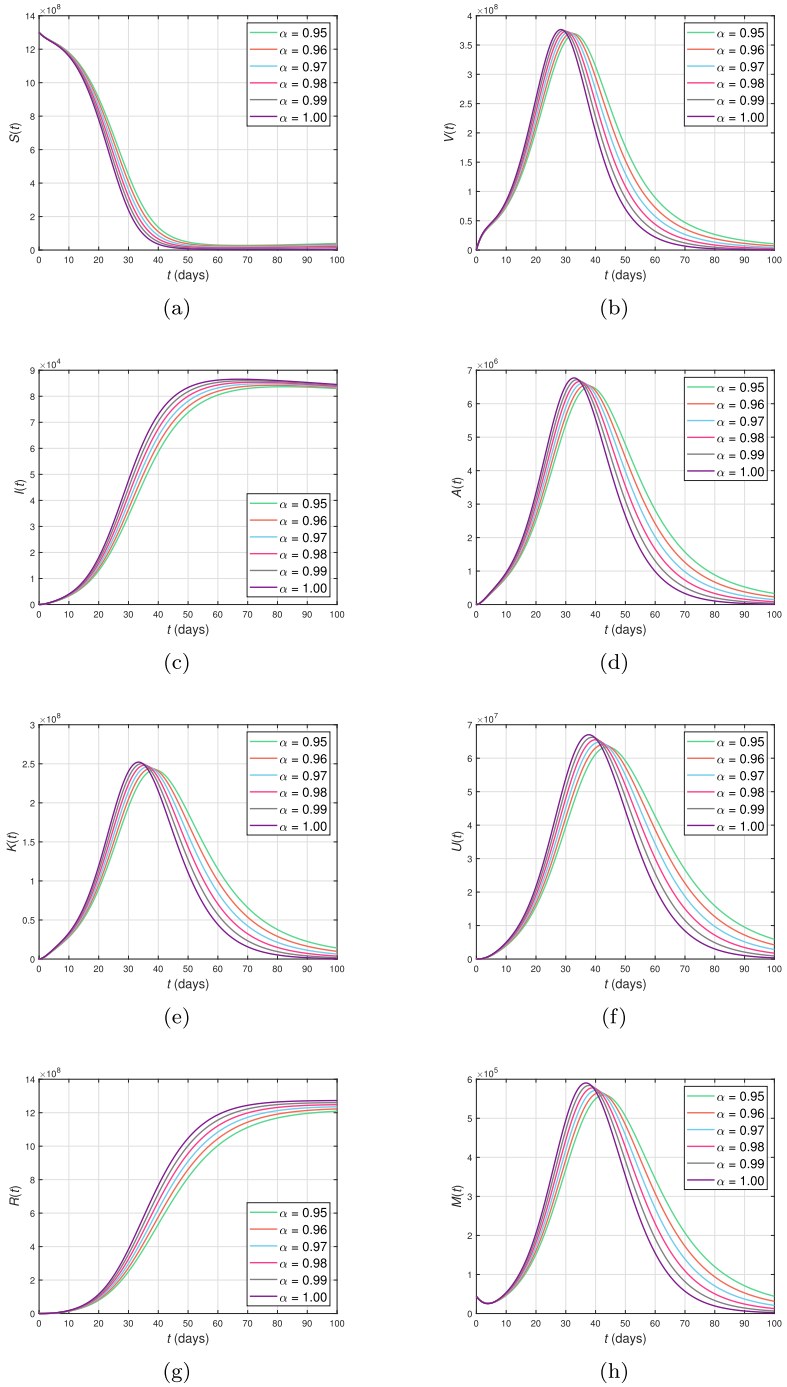

Fig. 2 The dynamics of the model (22) with a Mittag–Leffler kernel.

$$\int_0^{t_{k+1}} F(S(s))\mathrm{M_L}(t_{k+1}-s)\,ds \approx \sum_{j=0}^{k} d_{k+1,j}F(S_j), \tag{35}$$

where $d_{k+1,j} = \int_{t_j}^{t_{j+1}} \mathrm{M_L}(t_{k+1}-s)\,ds$. The predictor formula is then derived as the following equation

$$S_{k+1}^{p} = S_0 + \sum_{j=0}^{k} d_{k+1,j}F(S_j). \tag{36}$$

Finally, this method is repeated for the remaining equations in (22).

5. Results and discussion

Here, the general fractional model (22) is analyzed and investigated by applying the numerical method previously studied in Section 4. According to the COVID-19 real data from Wuhan (China), the values of parameters were extracted from [18] with respect to the following data-fitting analysis. The WHO reported that the total number of daily patients was 83249 by 3344 deaths between January 11, 2020, and April 19, 2020 [43,44]. Regarding this information and in order to parameter-

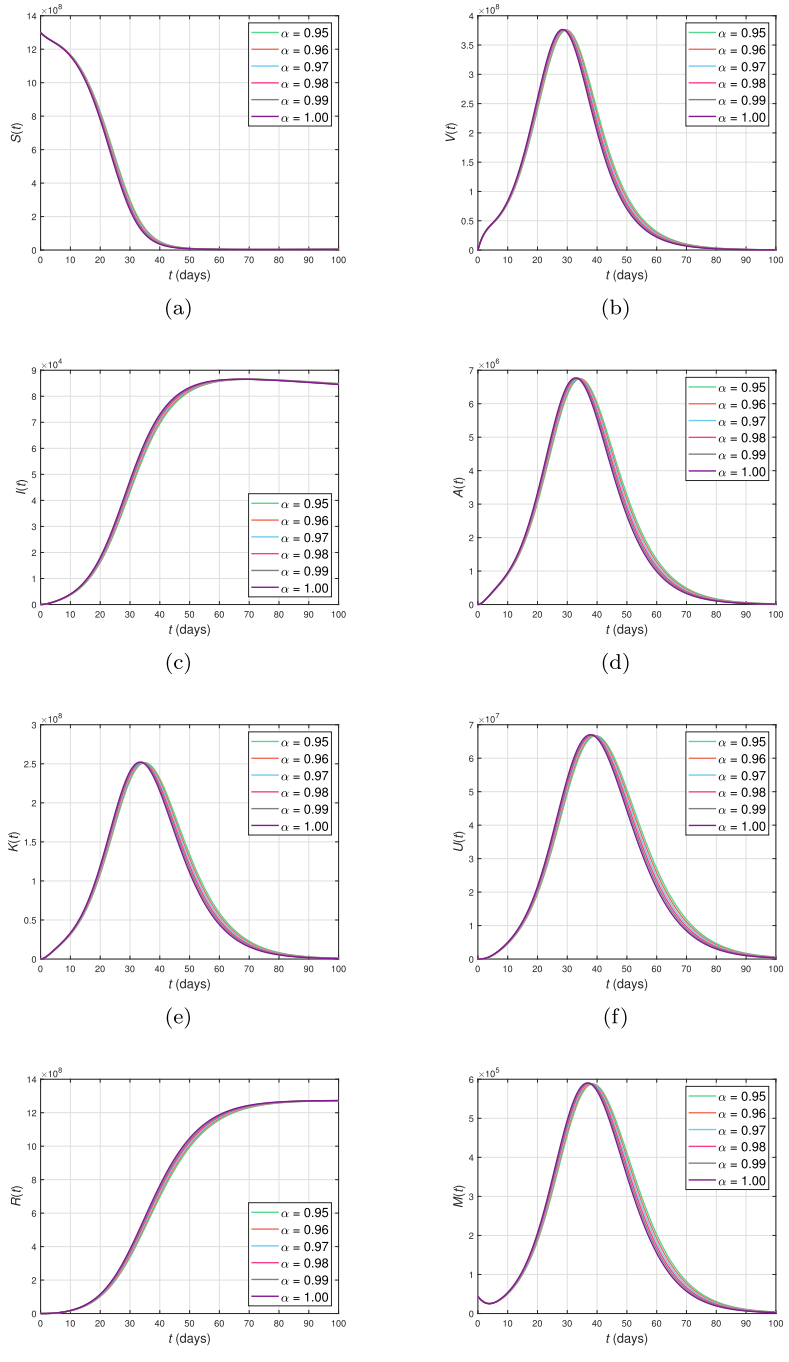

Fig. 3 The dynamics of the model (22) with an exponential kernel.

Table 2 Absolute and relative errors for the model (22) with a power law kernel.

Fractional-order	Absolute error	Relative error
0.95	5.7984×10^4	0.0866
0.96	5.0338×10^4	0.0752
0.97	4.4278×10^4	0.0662
0.98	4.0401×10^4	0.0604
0.99	3.9253×10^4	0.0587
1	4.0988×10^4	0.0612

Table 3 Absolute and relative errors for the model (22) with a Mittag–Leffler kernel.

Fractional-order	Absolute error	Relative error
0.95	7.5418×10^4	0.1127
0.96	6.2881×10^4	0.0940
0.97	5.2074×10^4	0.0778
0.98	4.3978×10^4	0.0657
0.99	3.9966×10^4	0.0597
1	4.0988×10^4	0.0612

ize the model (22), the fractional-order was fixed as $\alpha = 1$, and the model was simulated by applying the least-squares fitting technique. Table 1 shows the results that were determined realistically. According to the total China population, we also set $P(0) = 1,300,000,000$. Moreover, based on the number of cumulative cases, the infected individuals had an initial value of $I(0) = 4$, while the possible exposed cases were initialized at $V(0) = 20,000$. The value of $S(0) = 1,299,979,959$ was also estimated to be the susceptible population in the COVID-19 absence, whereas $M(0)$ was selected as $M(0) = 44,000$ from data fitting; the remaining compartments of the model were assumed to be zero at $t = 0$. According to these estimates, the mortality rate (per day) was obtained as $\xi = \frac{1}{76.79}$, while the birth rate (per day) was computed by $\beta = 46,381$. For the given time duration of infected cases, $R_0 \approx 6.6361$ was also estimated as the basic reproduction number. The time was measured in the unit of days, and the system (22) was simulated applying the power-law, Mittag–Leffler, and exponential kernels in Figs. 1–3, respectively. As a result, the general fractional derivative would present a flexible system, a fact which allows researchers to derive different aspects from the under-investigated system accurately. Tables 2–4 show the absolute and relative errors via using the power-law, Mittag–Leffler, and exponential kernels for different fractional orders, respectively. According to these results, one can see that the best fractional order is 0.99 for all three cases. Fig. 4 displays the fractional simulations by considering the (a) power-law, (b) Mittag–Leffler, and (c) exponential kernels versus the real reported cases of COVID-19 in China. The results illustrate

Table 4 Absolute and relative errors for the model (22) with an exponential kernel.

Fractional-order	Absolute error	Relative error
0.95	4.3620×10^4	0.0652
0.96	4.2339×10^4	0.0633
0.97	4.1430×10^4	0.0619
0.98	4.0904×10^4	0.0611
0.99	4.0760×10^4	0.0609
1	4.0988×10^4	0.0612

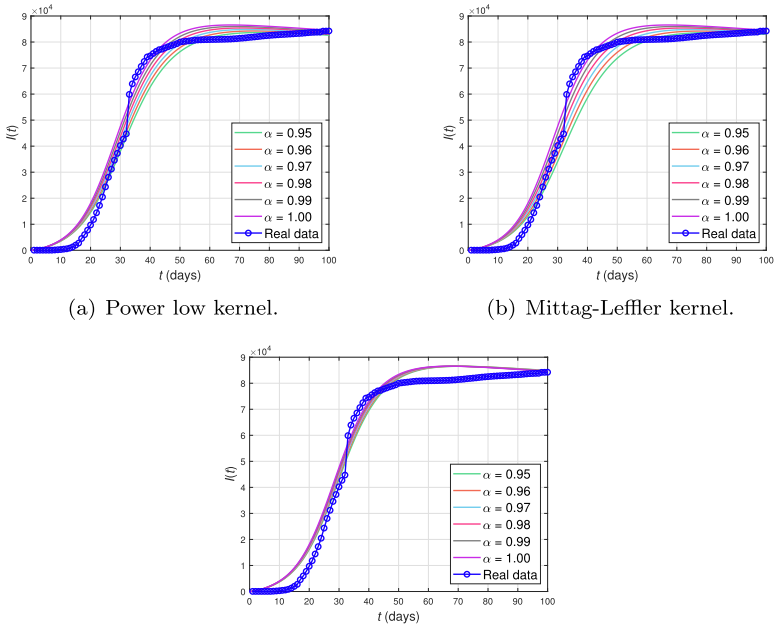

(a) Power low kernel.

(b) Mittag-Leffler kernel.

(c) Exponential kernel.

Fig. 4 Comparison of the three special fractional cases versus the real reported infected numbers in China.

the improvement which is made by applying the new general fractional model to follow the real data better than the classical integer-order model. Table 5 compares the absolute and relative errors for the integer-order model (15) and the three particular cases of fractional formula (22). This table indicates that the best solution is associated with the power-law kernel with the fractional order $\alpha = 0.99$, absolute error 3.9253×10^4, and relative error 0.0587. More to the point, the fractional results in all cases are better than the integer-order counterpart. Considering the most realistic case, *i.e.*, the fractional model (22) with a power-law kernel and $\alpha = 0.99$, we will examine the effect of some parameters on the system dynamics hereinafter. The amount of infected people for certain values is illustrated by θ_2. This amount declines very quickly when the infection rate in the seafood market decreases, as illustrated in Fig. 5a. Consequently, closing the seafood market could be a vital act by the Chinese government in order to prevent the infection from spreading further. Fig. 5b shows the proportion of the asymptomatic infection parameter ω graphically. The number of infected individuals decreases by a reduction in the value of ω. Thus, the asymptomatic infection plays a vital role in the infection development, so it is necessary to educate people about how to avoid contact with such individuals. Figs. 5c–e depict the effect

Table 5 Comparison of the three special fractional cases and the integer-order model.

Model	Fractional-order	Absolute error	Relative error
Fractional with a power law kernel	0.99	3.9253×10^4	0.0587
Fractional with a Mittag–Leffler kernel	0.99	3.9966×10^4	0.0597
Fractional with an exponential kernel	0.99	4.0760×10^4	0.0609
Integer-order	1	4.0988×10^4	0.0612

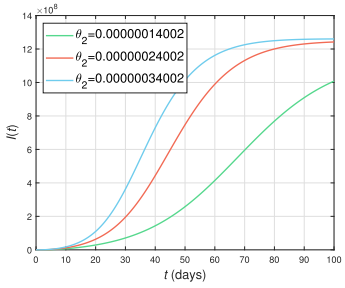

(a) Number of infected individuals for the various values of θ_2.

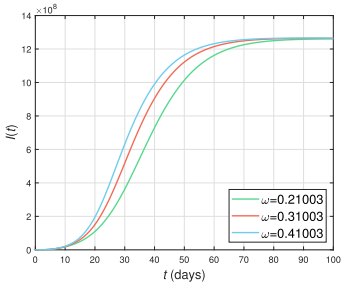

(b) Number of infected individuals for the various values of ω.

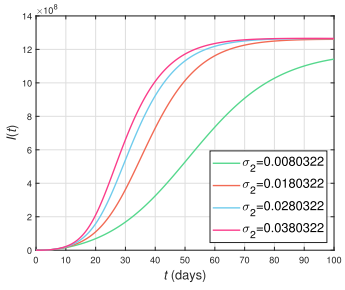

(c) Number of infected individuals for the various values of σ_2.

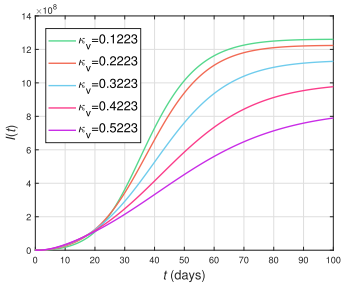

(d) Number of infected individuals for the various values of κ_v.

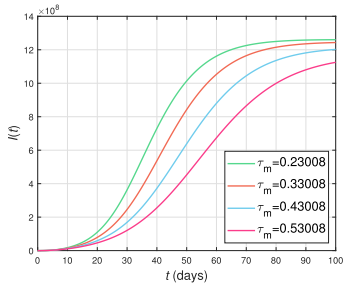

(e) Number of infected individuals for the various values of τ_m.

Fig. 5 The effect of parameters $\theta_2, \omega, \sigma_2, \kappa_v$, and τ_m on the number of infected individuals via the use of the fractional model (22) with a power-law kernel and $\alpha = 0.99$.

of parameters σ_2, κ_v, and τ_m, respectively. It could be obvious that the number of infected people decreases by the reduction of these parameters. Consequently, the quarantine class would be extremely crucial for the COVID-19 modelling.

6. Conclusions

This paper investigated a new fractional model of COVID-19 by considering the effects of isolation and quarantine. The model was first developed through ordinary time-derivatives and then modified by applying the general structure of fractional operators. The model stability was discussed, and the parameters were estimated based on a realistic situation in China, so the basic reproduction number was calculated as $R_0 \approx 6.6361$. Simulation results were obtained through an efficient numerical method used to solve the associated general fractional differential equations. As a result, some graphs and tables were provided for various fractional orders and different kernel functions. It was shown that a particular case of fractional model fits the reality more accurately than the other classical and fractional cases. Graphically, some other parameters with their effects on the model behavior were examined, which could act as the control for the disease eradication. Therefore, this study provides several important data that can help to eradicate the disease from communities as soon as possible. As a future study, other control methodologies such as those discussed in [45,46] could be examined in order to find out whether or not they can provide any positive impact on the control of COVID-19 pandemic.

Declaration of Competing Interest

The authors declare that they have no known competing financial interests or personal relationships that could have appeared to influence the work reported in this paper.

Acknowledgements

The research of JJN has been partially supported by Xunta de Galicia under grant ED431C 2019/02 and by Instituto de Salud Carlos III, grant COV20/00617.

References

[1] F. Brauer, C. Castillo-Chavez, Z. Feng, Mathematical Models in Epidemiology, Springer-Verlag, New York, 2019.
[2] R. Ratnayake, F. Finger, A.S. Azman, D. Lantagne, S. Funk, W.J. Edmunds, F. Checchi, Highly targeted spatiotemporal interventions against cholera epidemics, 2000–19: a scoping review, Lancet Infect. Dis. 21 (3) (2021) e37–e48.
[3] I. Area, F. Ndaïrou, J.J. Nieto, C.J. Silva, D.F.M. Torres, Ebola model and optimal control with vaccination constraints, J. Ind. Manag. Optim. 14 (2018) 427–446.
[4] H.M. Srivastava, I. Area, J.J. Nieto, Power-series solution of compartmental epidemiological models, Math. Biosci. Eng. 18 (2021) 3274–3290.
[5] C.J. Silva, C. Cruz, D.F.M. Torres, A.P. Muñuzuri, A. Carballosa, I. Area, J.J. Nieto, R. Fonseca-Pinto, R. Passadouro, E. Soares dos Santos, W. Abreu, J. Mira, Optimal control of the COVID-19 pandemic: controlled sanitary deconfinement in Portugal, Sci. Rep. 11 (2021) 3451.
[6] F. Ndaïrou, I. Area, J.J. Nieto, C.J. Silva, D.F.M. Torres, Fractional model of COVID-19 applied to Galicia, Spain and Portugal, Chaos Soliton. Fract. 144 (2021) 110652.
[7] S. Kumar, R.P. Chauhan, S. Momani, S. Hadid, Numerical investigations on COVID-19 model through singular and non-singular fractional operators, Numer. Methods Partial Differ. Equ. (2020), https://doi.org/10.1002/num.22707.
[8] Y.F. Lin, Q. Duan, Y. Zhou, et al, Spread and impact of COVID-19 in China: a systematic review and synthesis of predictions from transmission-dynamic models, Front. Med. 7 (2020) 321.
[9] G. Giordano, F. Blanchini, R. Bruno, P. Colaneri, A. Di Filippo, A. Di Matteo, M. Colaneri, Modeling the COVID-19 epidemic and implementation of population-wide interventions in Italy, Nat. Med. 26 (6) (2020) 855–860.
[10] T.A. Biala, A.Q.M. Khaliq, Fractional-order compartmental model for the spread of the COVID-19 pandemic, Commun. Nonlinear Sci. Numer. Simul. 98 (2021) 105764.
[11] J.F. Oliveira, D.C. Jorge, R.V. Veiga, et al, Mathematical modeling of COVID-19 in 14.8 million individuals in Bahia, Brazil, Nat. Commun. 12 (1) (2021) 333.
[12] O.J. Peter, S. Qureshi, A. Yusuf, M. Al-Shomrani, A.A. Idowu, A new mathematical model of COVID-19 using real data from Pakistan, Results Phys. 24 (2021) 104098.
[13] M.A. Khan, S. Ullah, S. Kumar, A robust study on 2019-nCOV outbreaks through non-singular derivative, Eur. Phys. J. Plus 136 (2) (2021) 168.
[14] D. Dwomoh, S. Iddi, B. Adu, J.M. Aheto, K.M. Sedzro, J. Fobil, S. Bosomprah, Mathematical modeling of COVID-19 infection dynamics in Ghana: impact evaluation of integrated government and individual level interventions, Infect. Dis. Model. 6 (2021) 381–397.
[15] A. Atangana, A novel COVID-19 model with fractional differential operators with singular and non-singular kernels: analysis and numerical scheme based on Newton polynomial, Alex. Eng. J. 60 (4) (2021) 3781–3806.
[16] S. Kumar, R. Kumar, S. Momani, S. Hadid, A study on fractional COVID-19 disease model by using Hermite wavelets, Math. Methods Appl. Sci. (2021), https://doi.org/10.1002/mma.7065.
[17] K.M. Safare, V.S. Betageri, D.G. Prakasha, P. Veeresha, S. Kumar, A mathematical analysis of ongoing outbreak COVID-19 in India through nonsingular derivative, Numer. Methods Partial Differ. Equ. 37 (2) (2021) 1282–1298.
[18] M.A. Khan, A. Atangana, E. Alzahrani, Fatmawati: The dynamics of COVID-19 with quarantined and isolation, Adv. Differ. Equ. 2020 (1) (2020) 425.
[19] J. Danane, K. Allali, Z. Hammouch, K.S. Nisar, Mathematical analysis and simulation of a stochastic COVID-19 Lévy jump model with isolation strategy, Results Phys. 23 (2021) 103994.
[20] T. Omay, D. Baleanu, Fractional unit-root tests allowing for a fractional frequency flexible Fourier form trend: predictability of COVID-19, Adv. Differ. Equ. 2021 (1) (2021) 167.
[21] M. Zamir, F. Nadeem, T. Abdeljawad, Z. Hammouch, Threshold condition and non pharmaceutical interventions's control strategies for elimination of COVID-19, Results Phys. 20 (2021) 103698.
[22] M.A. Noor, A. Raza, M.S. Arif, M. Rafiq, K.S. Nisar, I. Khan, S.F. Abdelwahab, Non-standard computational analysis of the stochastic COVID-19 pandemic model: An application of computational biology, Alex. Eng. J. 61 (1) (2022) 619–630.
[23] W. Gao, H.M. Baskonus, L. Shi, New investigation of bats-hosts-reservoir-people coronavirus model and application to 2019-nCoV system, Adv. Differ. Equ. 2020 (1) (2020) 391.
[24] H. Mohammadi, S. Rezapour, A. Jajarmi, On the fractional SIRD mathematical model and control for the transmission of COVID-19: the first and the second waves of the disease in Iran

and Japan, ISA Trans. (2021), https://doi.org/10.1016/j.isatra.2021.04.012.
[25] D. Baleanu, S.S. Sajjadi, A. Jajarmi, Ö. Defterli, J.H. Asad, The fractional dynamics of a linear triatomic molecule, Rom. Rep. Phys. 73 (1) (2021) 105.
[26] D. Baleanu, S.S. Sajjadi, A. Jajarmi, Ö. Defterli, On a nonlinear dynamical system with both chaotic and nonchaotic behaviors: a new fractional analysis and control, Adv. Differ. Equ. 2021 (1) (2021) 234.
[27] D. Baleanu, S.S. Sajjadi, J.H. Asad, A. Jajarmi, E. Estiri, Hyperchaotic behaviors, optimal control, and synchronization of a nonautonomous cardiac conduction system, Adv. Differ. Equ. 2021 (1) (2021) 157.
[28] D. Baleanu, S. Zibaei, M. Namjoo, A. Jajarmi, A nonstandard finite difference scheme for the modeling and nonidentical synchronization of a novel fractional chaotic system, Adv. Differ. Equ. 2021 (1) (2021) 308.
[29] M.A. Alqudah, C. Ravichandran, T. Abdeljawad, N. Valliammal, New results on Caputo fractional-order neutral differential inclusions without compactness, Adv. Differ. Equ. 2019 (1) (2019) 528.
[30] C. Ravichandran, J.J. Trujillo, Controllability of impulsive fractional functional integro-differential equations in Banach spaces, J. Funct. Spaces 2013 (2013) 812501.
[31] C. Ravichandran, K. Logeswari, F. Jarad, New results on existence in the framework of Atangana-Baleanu derivative for fractional integro-differential equations, Chaos Soliton. Fract. 125 (2019) 194–200.
[32] R. Subashini, K. Jothimani, K.S. Nisar, C. Ravichandran, New results on nonlocal functional integro-differential equations via Hilfer fractional derivative, Alex. Eng. J. 59 (5) (2020) 2891–2899.
[33] K.S. Nisar, K. Jothimani, K. Kaliraj, C. Ravichandran, An analysis of controllability results for nonlinear Hilfer neutral fractional derivatives with non-dense domain, Chaos Soliton. Fract. 146 (2021) 110915.
[34] Y. Luchko, M. Yamamoto, General time-fractional diffusion equation: some uniqueness and existence results for the initial-boundary-value problems, Fract. Calc. Appl. Anal. 19 (3) (2016) 676–695.
[35] O.P. Agrawal, Generalized variational problems and Euler-Lagrange equations, J. Comput. Appl. Math. 59 (5) (2010) 1852–1864.
[36] I. Podlubny, Fractional Differential Equations: An Introduction to Fractional Derivatives, Fractional Differential Equations, to Methods of Their Solution and Some of Their Applications, Academic Press, New York, 1998.
[37] A. Atangana, D. Baleanu, New fractional derivatives with nonlocal and non-singular kernel: Theory and application to heat transfer model, J. Therm. Sci. 20 (2) (2016) 763–769.
[38] M. Caputo, M. Fabrizio, A new definition of fractional derivative without singular kernel, Prog. Fract. Differ. Appl. 1 (2) (2015) 73–85.
[39] M. Caputo, M. Fabrizio, On the singular kernels for fractional derivatives. Some applications to partial differential equations, Prog. Fract. Differ. Appl. 7 (2) (2021) 79–82.
[40] J. Losada, J.J. Nieto, Fractional integral associated to fractional derivatives with nonsingular kernels, Prog. Fract. Differ. Appl. 7 (3) (2021) 137–143.
[41] J.F. Gómez-Aguilar, J.J. Rosales-García, J.J. Bernal-Alvarado, T. Córdova-Fraga, R. Guzmán-Cabrera, Fractional mechanical oscillators, Rev. Mex. de Fis. 58 (2012) 348–352.
[42] P. Van den Driessche, J. Watmough, Reproduction numbers and sub-threshold endemic equilibria for compartmental models of disease transmission, Math. Biosci. 180 (1–2) (2002) 29–48.
[43] World Health Organization (WHO). https://who.sprinklr.com/region/wpro/country/cn.
[44] Wuhan, China Population 1950-2020. https://www.macrotrends.net/cities/20712/wuhan/population.
[45] A. Jajarmi, N. Pariz, S. Effati, A.V. Kamyad, Infinite horizon optimal control for nonlinear interconnected large-scale dynamical systems with an application to optimal attitude control, Asian J. Control 14 (5) (2012) 1239–1250.
[46] S. Effati, H.S. Nik, A. Jajarmi, Hyperchaos control of the hyperchaotic Chen system by optimal control design, Nonlinear Dyn. 73 (1–2) (2013) 499–508.